Characterization of the Binding of Isoniazid and Analogues to *Mycobacterium tuberculosis* Catalase-Peroxidase†

Xiangbo Zhao,‡,§ Shengwei Yu,‡ and Richard S. Magliozzo*,‡,§

Department of Chemistry, Brooklyn College, Brooklyn, New York 11210, and Department of Biochemistry, The Graduate Center of The City University of New York, New York, New York 10016

Received October 25, 2006; Revised Manuscript Received January 11, 2007

ABSTRACT: The first-line antituberculosis drug isonicotinic hydrazide (INH) is a prodrug whose bactericidal function requires activation by *Mycobacterium tuberculosis* catalase-peroxidase (KatG) to produce an acyl-NAD adduct. Peroxidation of INH is considered a required catalytic process for drug action. The binding of INH and a series of hydrazide analogues to resting KatG was examined using optical and calorimetric techniques to provide thermodynamic parameters, binding stoichiometries, and kinetic constants (on and off rates). This work revealed high-affinity binding of these substrates to a small fraction of ferric enzyme in a six-coordinate heme iron form, a species most likely containing a weakly bound water molecule, which accumulates during storage of the enzyme. The binding of hydrazides is associated with a large enthalpy loss (>100 kcal/mol); dissociation constants are in the range of 0.05−1.6 μM, and optical stopped-flow measurements demonstrated k_{on} values in the range of 0.5−27 × 10^3 M^{-1} s^{-1} with very small k_{off} rates. Binding parameters did not depend on pH in the range 5−8. High-affinity binding of INH is disrupted in two mutant enzymes bearing replacements of key distal side residues, KatG[W107F] and KatG[Y229F]. The rates of reduction of KatG Compound I by hydrazides parallel the on rates for association with the resting enzyme. In a KatG-mediated biomimetic activation assay, only isoniazid generated in good yield the acyl-NAD adduct which is considered a key molecule in INH action, providing a better understanding of the action mechanism of INH.

Isonicotinic hydrazide (INH,[1] isoniazid) has been used as a first-line antituberculosis drug since the 1950s (*1*). However, its cellular targets and its mechanism of action remain topics of continued interest and research. INH is a prodrug requiring activation by *Mycobacterium tuberculosis* (*Mtb*) catalase-peroxidase (KatG) (*2*). *Mtb* KatG is a bifunctional heme enzyme whose catalytic cycles involve formation of the reactive oxoferryl heme π-cation radical intermediate, Compound I, upon reaction with peroxides. Compound I is catalytically competent in the reaction with INH and other substrates (*3*). KatG Compound I was also found to rapidly decay in the absence of reducing substrates, during which protein-based tyrosyl and tryptophanyl radicals are formed (*4*−*6*). The drug also quenches amino acid-based radicals, though the relative importance of this reaction in drug activation is not known. In vitro studies showed that in the presence of a slow flux of H_2O_2 or superoxide, KatG converts INH into a radical species that can subsequently acylate nicotinamide adenine dinucleotide cofactor to form an INH−NAD(P) adduct (*7*−*11*). The INH−NAD adduct is a potent inhibitor of *Mtb* InhA, an enoyl reductase required for the elongation steps in mycolic acid biosynthesis (*12*−*14*). These acids are key components of the mycobacterial cell wall, and the inhibition of InhA is considered central to INH action against *Mtb*. The INH−NADP adduct was recently found to be an inhibitor of *Mtb* dihydrofolate reductase (*15*).

An analysis of the interactions between organic donor molecules such as aryl hydrazides and KatG is of interest in part because binding of specific small molecules to heme peroxidases has only been characterized in detail for a few examples. INH binding is particularly interesting due to the fact that the reduced affinity for INH in the KatG[S315T] mutant has been shown to account for drug resistance in strains carrying this mutant enzyme (*10*, *16*). Characterization of an INH binding site in KatG has been experimentally and theoretically approached; both methods suggest that specific binding occurs within the heme pocket on the distal side (*17*−*19*). While KatG structures from several sources have been determined during the past few years (*10*, *20*−*22*), these studies have not yet yielded a structure of a KatG−INH complex. This lack presents a challenge in understanding and defining INH activation.

Changes in the absorption spectrum of resting KatG provided evidence of binding of INH to the resting enzyme, which results in a class I spectral change consistent with a

† This work was supported by National Institutes of Health Grant AI-060014 (National Institute of Allergy and Infectious Diseases) and PSC-CUNY Grant 66404-0035 to R.S.M.

* To whom correspondence should be addressed: Department of Chemistry, Brooklyn College, 2900 Bedford Ave., Brooklyn, NY 11210. Telephone: (718) 951-5000, ext. 2845. Fax: (718) 951-4607. E-mail: rmaglioz@brooklyn.cuny.edu.

‡ Brooklyn College.

§ The Graduate Center of The City University of New York.

[1] Abbreviations: *Mtb*, *Mycobacterium tuberculosis*; KatG, catalase-peroxidase; ITC, isothermal titration calorimetry; HRP, horseradish peroxidase; EPR, electron paramagnetic resonance; INH, isonicotinic acid hydrazide; NH, nicotinic acid hydrazide; FRH, furoic hydrazide; BZH, benzoic hydrazide; PNH, picolinic hydrazide; PyNH, 1-*H*-pyrrol-2-carbohydrazide; BHA, benzhydroxamic acid; PAA, peroxyacetic acid.

10.1021/bi062218p CCC: $37.00
Published on Web 02/20/2007

shift from six-coordinate (6-c) to five-coordinate (5-c) heme iron (*18*, *23*). KatG isolated from *Mtb* cells exhibits a mixture of 5-c and 6-c heme (*23*), and heme heterogeneity is also found in overexpressed recombinant KatG isolated from *Escherichia coli* (*18*, *24*). More interestingly, the heme iron of freshly isolated recombinant *Mtb* KatG is predominantly 5-c, while a 6-c species accumulates during storage of the purified enzyme (*24*). Such changes in heme iron coordination could be evidence of the modification in the microenvironment of the heme pocket and/or of more remote structural changes that affect the distal side architecture. The specific origin of these changes is not yet understood, though this study demonstrates their impact on INH binding.

Other questions relating to the stoichiometry, thermodynamics, and kinetics of INH binding are essential for gaining an understanding of the KatG-mediated activation mechanism for this prodrug. To address these unreported but important issues, we examined the binding of INH and analogues to KatG using a combination of isothermal titration calorimetry (ITC), spectroscopic, and mutagenesis approaches. We demonstrate that for wild-type KatG, the INH binding stoichiometry is relatively low, with high-affinity binding to only the form of enzyme in which 6-c iron has formed. Issues concerning turnover of INH and other hydrazides by KatG are also investigated here.

EXPERIMENTAL PROCEDURES

Materials. E. coli UM262 containing the *Mtb katG* gene in pKAT II was a gift from S. Cole (Institut Pasteur, Paris, France). KatG[W107F] and KatG[Y229F] mutants were constructed according to previously described procedures (*25*). 1-*H*-Pyrrol-2-carbohydrazide was purchased from Interchim (Montlucon, France). All other reagents were from Sigma-Aldrich. Commercial peroxyacetic acid was treated with bovine liver catalase to remove hydrogen peroxide. INH was recrystallized from methanol, and solutions were freshly prepared for each experiment to avoid complications due to hydrolysis and/or autoxidation (*26*). Other chemicals were used as supplied and were of the highest available purity.

KatG Overexpression and Purification. Mtb KatG and the mutant enzymes were expressed and purified as previously described (*3*). Purified KatG was dissolved in 20 mM phosphate buffer (pH 7.2), and the active protein concentration is reported as the heme concentration evaluated using the pyridine hemochromogen method (*27*).

Isothermal Titration Calorimetry. Experiments were carried out using a VP-ITC calorimeter (Microcal) at 25 °C in phosphate buffer (pH 7.2). KatG and hydrazide solutions were equilibrated with nitrogen for $^1/_2$ h and were degassed under vacuum before titration. Multiple injections (4−6 μL each) of a hydrazide solution (0.1−0.2 mM) were added to a KatG (10 μM) solution in the sample cell under continuous stirring. The slow changes in signals (microcalories per second) required long intervals between each injection, which ranged between 300 and 720 s depending on the hydrazide. Data were analyzed for binding stoichiometry, dissociation constant, and other thermodynamic parameters using Origin by integrating raw data (heat pulse in microcalories per second per injection) and fitting to a standard single-site binding model. Control titrations showed that the heat of dilution for hydrazide was very small and therefore could be ignored in data processing.

Optical Difference Spectrophotometric Titration. Optical titrations of KatG (freshly prepared or after storage for brief periods) with hydrazides were carried out anaerobically in a sealed cuvette to prevent potential aerobic reactions that could interfere with measurements, including the spontaneous or enzyme-catalyzed decomposition of hydrazide. [Prior work suggests that autocatalytic processes can occur in aerobic mixtures of resting KatG and INH due to endogenous peroxide formation (*28*).] KatG and hydrazide solutions were purged with nitrogen for 30 min before titration. Aliquots (2 μL each) of 0.5 mM hydrazide were added to the sample (5 μM KatG, 2 mL) as well as the reference cuvette with the same total volume of solution in each. To reach saturation, a concentrated hydrazide solution was used to minimize volume changes toward the end of the titration. Spectra of KatG were recorded after the optical change was complete for each addition (15 min for INH, otherwise 5 min). Difference spectra were obtained by subtracting the spectrum of the starting KatG sample from the spectrum recorded after addition of each aliquot. Titration curves were created by plotting $\Delta A_{\text{peak-trough}}$ values from the difference spectra versus the molar ratio of added hydrazide (*23*).

Kinetics of Hydrazide Binding. The kinetics of binding of hydrazide to KatG was determined using a diode-array stopped-flow spectrophotometer (Hi-Tech Scientific model SF-61 DX2). An equal volume of hydrazide and KatG (enzyme used here had sufficient 6-c form to allow adequate measurement of accurate absorbance changes upon hydrazide binding) was mixed at 25 °C in phosphate buffer (pH 7.2). The final concentration of KatG was 5 μM. For each hydrazide, various concentrations ranging from 50 to 400 μM were used to establish linear plots of rates (k_{obs}) versus concentration. The decrease in absorbance of KatG at 412 nm (wavelength of maximum difference between the initial and final absorbance in the Soret region) was fit to a single-exponential function. The apparent association rate constants (k_{on}) for hydrazide binding were obtained from the slope of the linear dependence of k_{obs} on concentration. The dissociation rate constants (k_{off}) were the values of the *y*-intercepts of the linear plots of k_{obs}.

Reaction of Hydrazides with KatG Compound I. Reduction of KatG Compound I by hydrazides was followed using double-mixing stopped-flow spectophotometry according to the method of Yu et al. (*16*). Briefly, KatG was treated with a small excess of peroxyacetic acid (PAA, H_2O_2-free) in the first mixing step. Hydrazide was subsequently added after a 2 s delay. Final concentrations of KatG, PAA, and hydrazide were 5, 50, and 50 μM, respectively. Spectra were recorded for 150 s beginning immediately after the addition of hydrazide.

Formation of the Hydrazide−NAD Adduct. The KatG-mediated formation of the hydrazide−NAD adduct was monitored according to a previously published protocol using a slow flux of hydrogen peroxide as an oxidant (*10*). Briefly, KatG, NAD^+, and INH were co-incubated with a glucose/glucose oxidase system, and the optical absorbance at 326 nm was used to detect formation of hydrazide−NAD adducts. We assume that all hydrazide−NAD analogues have similar extinction coefficients at 326 nm (*9*, *14*).

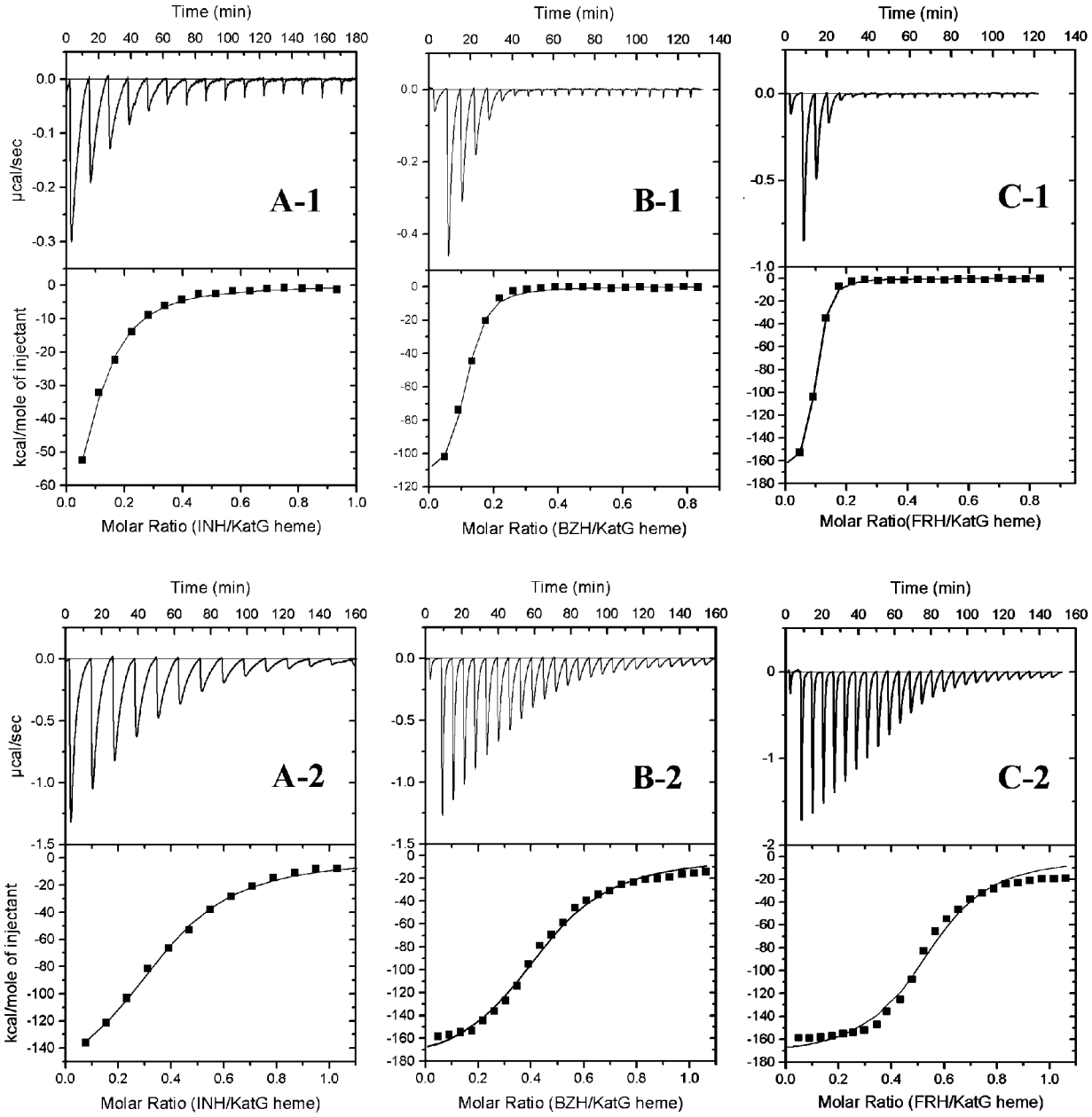

FIGURE 1: Isothermal titration of fresh and aged KatG with hydrazide ligands. ITC experiments were carried out at 25 °C in phosphate buffer (pH 7.2) using 10 μM KatG. The top panels show the isothermal traces and integrated heat signals measured from a series of injections of INH (A-1), BZH (B-1), or FRH (C-1) into freshly purified KatG. Heat signals (integrated values in microcalories per second per injection) are fitted to a single-binding site model. Bottom panels (A-2, B-2, and C-2) show the results using the KatG enzyme that had been stored for 3 weeks at 4 °C.

RESULTS

ITC Analysis of Binding of Hydrazide to Wild-Type KatG. Isothermal titration calorimetry monitors the heat evolved during the titration of the enzyme with substrate and provides a convenient way of determining the binding stoichiometry and thermodynamic parameters. In this study, INH and the structurally related analogues benzoic hydrazide (BZH) and furoic hydrazide (FRH) were utilized to gain a better understanding of the characteristics of binding of aromatic hydrazide to ferric KatG.

Freshly isolated recombinant *Mtb* KatG as routinely prepared and as described in previous reports (*24*, *29*) contains 5-c heme iron as a majority species and a small proportion (~10%) of 6-c heme. ITC experiments were performed using KatG within 2 days of purification (*24*). To prevent interference from potential oxygen-dependent reactions such as INH autoxidation, solutions were degassed prior to titration. Results of a typical titration of fresh KatG with INH, BZH, or FRH are shown in Figure 1 (top panels). The isothermal curves approached apparent saturation at a hydrazide concentration far less than 1 equiv/heme and even less than 0.5 or 1 equiv per KatG dimer; this phenomenon was more evident with BZH and FRH due to the higher affinity of KatG for these analogues. The integrated enthalpy changes were best fit to a single-binding site model, and parameters are given in Table 1. The *n* value, which is the apparent binding stoichiometry for substrate, is surprisingly low ($n \sim 0.1$ per monomer of KatG) in each case and corresponds to the concentration of the 6-c form of the enzyme estimated according the position of optical absorption

Table 1: Stoichiometries and Thermodynamics for Binding of Hydrazide to Freshly Prepared and Aged *Mtb* KatG As Determined by ITC

enzyme	substrate	n^a	K_d (μM)	ΔH (kcal/mol)	ΔS (kcal mol^{-1} K^{-1})
fresh KatG	INH	0.09 ± 0.01	1.37 ± 0.13	−112 ± 12	−0.35
	BZH	0.10 ± 0.01	0.12 ± 0.02	−165 ± 38	−0.37
	FRH	0.12 ± 0.02	0.05 ± 0.02	−176 ± 25	−0.54
aged KatG	INH	0.34 ± 0.03	1.61 ± 0.11	−177 ± 21	−0.56
	BZH	0.44 ± 0.03	0.14 ± 0.03	−129 ± 1	−0.41
	FRH	0.48 ± 0.04	0.07 ± 0.01	−192 ± 15	−0.61

[a] *n* is the apparent binding stoichiometry (moles of ligand per mole heme) obtained by fitting isothermal curves to a single-binding site model.

maxima for KatG used here, and correlations with previously published results (*30*).

For each substrate, dissociation constants were in the low micromolar range (Table 1). FRH had the highest affinity ($K_d \sim 0.07$ μM). The broad isothermal peaks indicate the slow binding of these substrates; INH binding was much slower than that of FRH or BZH. However, even the binding of FRH or BZH is ~3 times slower than rates seen in related experiments with horseradish peroxidase (HRP) binding with benzhydroxamic acid (BHA) (*31*).

Another notable feature of these titrations is that a significant enthalpy loss (>100 kcal/mol) was consistently observed. To probe whether catalytic turnover of the substrate in reactions requiring oxygen contributed to this, titrations were conducted using aerobic solutions, and also with addition of Mn^{2+} to stimulate known oxidative reactions (*28*). Such reactions produce superoxide and peroxide and can thereby initiate peroxidase turnover of substrates by KatG. No significant differences in the titrations under these conditions were found. Thus, enzymatic activity is unlikely to be a source of heat in the ITC experiments.

ITC titrations were then performed using KatG in which 6-c heme was more abundant. Previous studies have shown that storage of the purified enzyme at 4 °C for a few weeks does not diminish the specific activity but does produce an enrichment of the 6-c heme iron form (30% or more of the total heme species) (*24*). According to EPR spectroscopy and X-ray crystallography (*10*, *24*), the sixth ligand in this species is likely a molecule of water weakly bound to heme iron. As shown in Figure 1 (bottom panels, A-2, B-2, and B-3), titration curves now exhibited *n* values ranging from 0.34 to 0.48 mol of hydrazide/mol of heme (Table 1). Notably, the values of the calculated dissociation constants were not significantly different between the fresh and "aged" enzyme, consistent with homologous structural changes whether these occurred before or after the storage of the purified enzyme.

ITC experiments performed at pH 5.5 or 8.5 did not show a significant change in dissociation constant or binding stoichiomerty for the aged protein, compared to the results at pH 7.2 described above. ITC studies were also carried out in the presence of CN^- and F^-. The strong field ligand CN^- effectively inhibited hydrazide binding when added in a 20-fold excess, while for F^-, a very large excess was required for a similar effect. Though INH does not coordinate to heme iron, its binding was disfavored when a high-affinity ligand was bound to the heme iron.

Optical Difference Titrations of Fresh and Aged Wild-Type KatG. Changes in the KatG optical spectrum upon INH binding were first reported by Wengenack et al. (*18*). Here we focused mainly on revealing differences between freshly prepared and aged enzyme to relate optical behavior with the ITC results. Again, to avoid possible autoxidation reactions, and potential heme-catalyzed reactions, optical titrations were performed anaerobically in septum-sealed cuvettes. Freshly prepared KatG has a Soret peak at 405 nm and a CT1 band at 642 nm, consistent with the majority species being 5-c heme iron. These features change during storage; for example, in 2−3 days, the Soret peak and CT1 band were found at 406 and 637 nm, respectively. After the sample had been stored for 3 weeks at 4 °C, those bands were at 407/408 and 629 nm, respectively, which are close to their positions in the KatG enzyme used by Wengenack et al. (*18*, *23*) and consistent with the accumulation of 6-c heme iron (*24*). (The absorption spectra of fresh and aged KatG are provided as Supporting Information.)

Difference spectra collected during titration of KatG with INH exhibited a type I change in which the peak and trough were at 378−380 and 412−414 nm, respectively. Saturation with INH, BZH, or FRH caused a similar range of optical difference in each case (Figure 2, left panels). However, in titrations using aged enzyme, the magnitude of the optical change increased by ~3-fold. These observations are consistent with the fact that 6-c heme is more abundant in the aged enzyme and also has a higher Soret band extinction coefficient than the 5-c form. Whereas the titration curve for fresh KatG reached an apparent plateau with only 0.3 equiv of INH or its analogues per heme (Figure 2, right panels), here the saturation plateau occurred at approximately 0.8−1.0 equiv of hydrazide. If all enzyme forms had a similar affinity for INH, at least 1 equiv of substrate would be required to achieve saturation in all cases even though only the 6-c to 5-c transition produces an optical change, as all enzyme forms would be available for binding.

The time course of the optical changes in the case of INH was much slower than for the other molecules so that an equilibration time of 15 min was needed after addition of each INH aliquot. This is similar to the time for equilibration during ITC titration (see below). The kinetics of INH binding is described further below.

Determination of K_d values from the optical titration data requires knowledge of the total available binding sites. Our ITC studies provide a good estimation of the titratable KatG concentration. With an adjustment for total available sites assumed to be the "*n*" value estimated from the ITC results, the K_d for INH was estimated to be 1.0 μM (for the data in Figure 2, A-2), which is close to the value obtained from ITC experiments (~1.6 μM).

Results for BZH and FRH were similar to those for INH. Optical titration results parallel the ITC results, consistent with high-affinity binding to only a fraction of total enzyme, a 6-c form.

KatG[Y229F] and KatG[W107F] Mutants. The distal side of the heme pocket in KatG contains a three-residue covalent adduct involving the side chains of Y229, Trp107, and Met255 (*21*, *22*, *32*). To evaluate whether replacement of distal side residues has an impact on INH binding, mutant

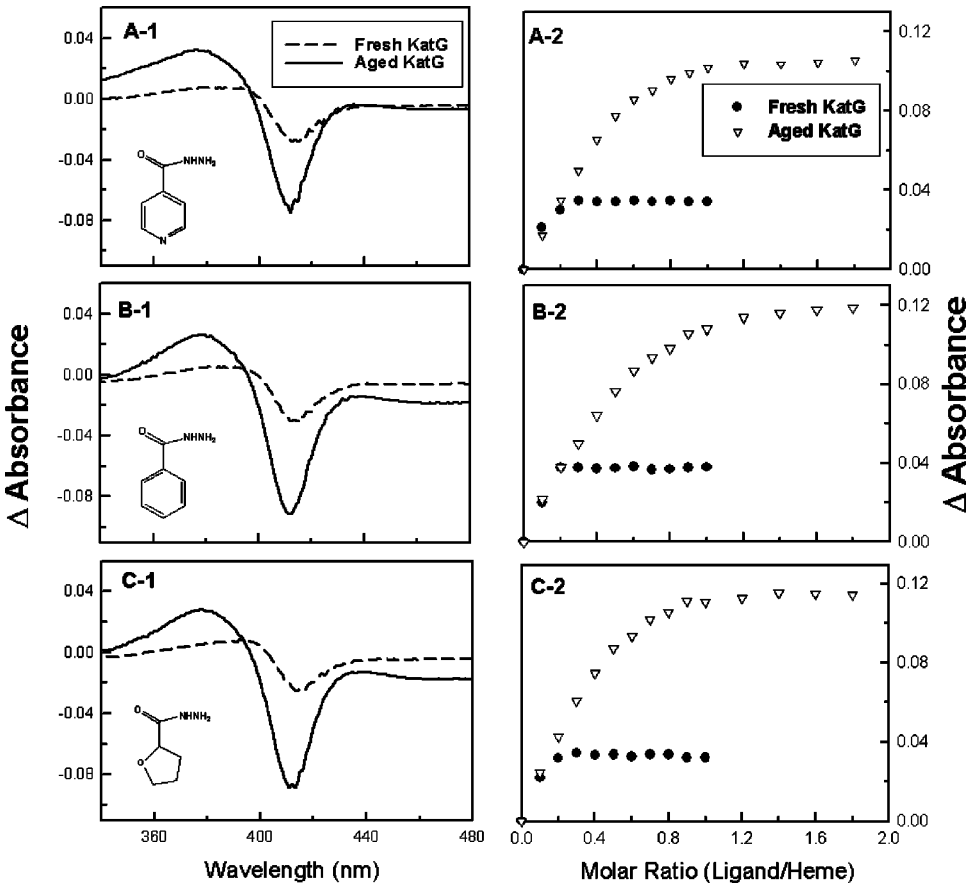

FIGURE 2: Optical titration of fresh and aged KatG with hydrazide ligands. Titrations were performed anaerobically using 5 μM enzyme with three structurally similar ligands: INH (A), BZH (B), and FRH (C). Hydrazide-induced difference spectra for fresh and aged KatG (left). Difference spectra were obtained by subtracting the spectrum of free KatG from that of the hydrazide-saturated enzyme. Hydrazide binding curves with fresh and "aged" KatG (right). Plots were generated by plotting the difference spectra (ΔA, peak absorbance minus trough absorbance) vs the molar ratio of ligand to KatG heme (monomer).

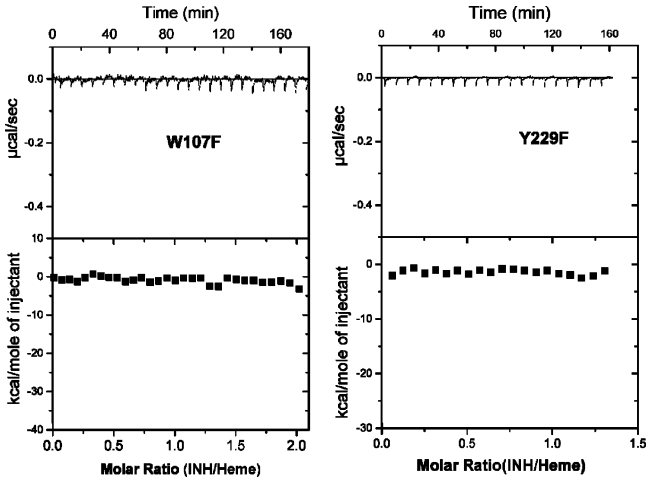

FIGURE 3: Isothermal titration of KatG[W107F] and KatG[Y229F] mutants with INH. Experimental conditions were the same as in Figure 1 using 10 μM overexpressed mutant proteins that had been stored at 4 °C for 2−3 weeks. The featureless isothermal curves are consistent with a lack of high-affinity binding for the mutants.

enzymes KatG[Y229F] and KatG[W107F] were used in ITC studies under the same conditions that were used for wild-type KatG. As shown in Figure 3, the binding enthalpy was barely detectable for these mutants even beyond the range of molar ratios used in the case of WT KatG (excess hydrazide), and no attempts were made to estimate binding parameters. Freshly prepared samples of both mutant enzymes behaved the same as samples stored for 2−3 weeks. Unlike wild-type KatG, no obvious optical spectral changes were observed in either mutant when INH titration experiments were performed (anerobically) using an up to 50-fold molar excess of INH. Thus, high-affinity binding of INH is disrupted in these two mutant enzymes.

Kinetics of Binding of Hydrazide to Wild-Type KatG. In both ITC and optical titrations, the process of INH binding was found to be very slow. We thought it was important to demonstrate whether the evolution of heat in ITC titrations corresponded to the same phenomenon as that causing the optical changes described above. Parallel experiments were carried out to compare the kinetics of isothermal titration and the time course of the spectral change upon addition of INH. To accelerate the mixing and minimize recording dead time, a stopped-flow spectrophotometer was used to collect the optical data. Comparison of results shows that addition of 0.2 equiv of INH to KatG produced a rate of optical change (decrease in A_{412}) matching the related step during isothermal titration calorimetry (Figure 4). The total time required for reaching equilibrium in both cases is essentially equal (~15 min). Thus, the heat released (microcalories per second) and the optical changes during this process apparently correspond to the same phenomena associated with INH binding.

The optical stopped-flow method was extended to evaluate the binding rate constants for various hydrazides under pseudo-first-order conditions. Values for k_{obs} were obtained

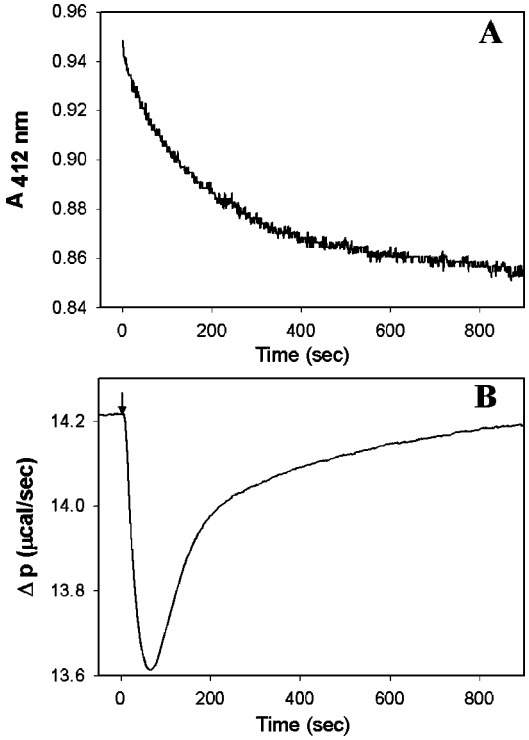

FIGURE 4: Slow binding of INH to KatG evidenced by optical and isothermal changes. (A) Representative stopped-flow spectrophotometric trace of KatG upon mixing with INH as measured by the decrease in absorbance at 412 nm. The final concentrations of KatG and INH were 10 and 2 μM, respectively. (B) Isothermal titration of KatG with INH. The arrow indicates the point on the baseline during titration at which 10 μL of INH (280 μM) was injected into the sample cell (containing 1.4 mL of 10 μM KatG). Thus, the final concentrations of KatG and INH in the sample cell were the same as in panel A. The injection time is 10 s (1 μL/s).

by fitting the traces of A_{412} versus time to a single-exponential function using KinetAsyst. The k_{obs} values exhibited a linear dependence on hydrazide concentration and fit the general equation for ligand binding:

$$k_{obs} = k_{on}[L] + k_{off}$$

Plots of k_{obs} values as a function of hydrazide concentration were generated to obtain slopes that provide second-order association rate constants (k_{on}). As shown in Table 2, the rates for INH and NH are much slower than those for the other molecules. Furthermore, the INH association rate constant is at least 2 orders of magnitude lower than typical enzyme−substrate binding rates, which are usually in the range of 10^4−10^5 M^{-1} s^{-1} (*33*). Ring size and other factors such as hydrophobicity strongly affect the rates, as FRH binding is 50 times faster than INH binding ($k_{on} = 27.7 \times 10^3$ and 0.48×10^3 M^{-1} s^{-1}, respectively) and 10 times faster than 1-*H*-pyrrol-2-carbohydrazide binding (PyHZ). The on rates also depended on the position of the hydrazide group in the pyridine-containing hydrazides. For example, picolinic hydrazide (PNH) had a faster binding rate compared to the nicotinic or isonicotinic forms, while the benzylic ring gave a significant increase in rate compared to the pyridine group. This is consistent with slow desolvation of the ring nitrogen as a possible contributing factor in the rate. For the five-membered rings, an oxygen atom at the meso position (as in FRH) greatly facilitated the binding compared to a protonated nitrogen at the same position (as in PyHZ). PNH and PyHZ, closely related in structure except for ring size, exhibited very similar binding rates. Apparently, the great gain in rate that would be expected for five- versus six-membered rings is lost due to the extra steric interference of the H atom on the ring nitrogen of PyHZ.

Table 2: Association and Dissociation Rate Constants for Binding of Hydrazide to KatG As Determined by Stopped-Flow Spectrophotometry

Hydrazide	STRUCTURE	k_{on} (10^3 $M^{-1}s^{-1}$) [a]	k_{off} (10^{-2} s^{-1}) [a]
Isoniazid (INH)	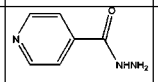	0.48 ± 0.02	2 ± 0.3
Nicotinic hydrazide (NH)	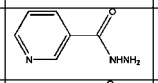	0.67 ± 0.02	0.3 ± 0.2
Picolinic hydrazide (PNH)	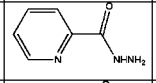	2.08 ± 0.04	0.3 ± 0.1
1-H-pyrrol-2-carbohydrazide (PyHZ)	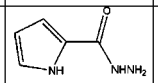	1.93 ± 0.10	1 ± 0.1
Benzoic hydrazide (BZH)	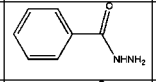	9.50 ± 0.57	2 ± 1
Furoic hydrazide (FRH)	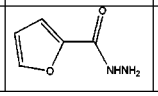	27.68 ± 0.77	4 ± 3

[a] On rates (k_{on}) and off rates (k_{off}) of hydrazide binding were determined by stopped-flow spectrophotometry following the decrease in A_{412} as described in Experimental Procedures. Rates are expressed as the means ± the standard deviation from triplicate analyses.

The dissociation rate constants (k_{off}) calculated from the *y*-intercepts of the linear plots of k_{obs} are very small with most in the range of 10^{-2} s^{-1}. The fitting errors for k_{off} are notable since the k_{off} is much smaller than the k_{obs} for these high-affinity substrates. Thus, unreliable K_d values would be obtained from the ratio k_{off}/k_{on}.

Reduction of KatG Compound I by Hydrazides. Additional kinetic experiments were designed to examine whether binding phenomena with the resting enzyme correlated with rates of reaction required for activation of INH through peroxidase catalysis by KatG Compound I. Double-mixing stopped-flow spectrophotometric experiments were carried out in which KatG was premixed with a small excess of peroxyacetic acid, which yields Compound I within 1 s in the first mixing step (*16*), followed by addition of hydrazides that reduce Compound I in a second mixing step. Ultimately, heme iron in the enzyme returns to the ferric state. [While tyrosyl and tryptophanyl radicals may also form under these conditions and may also react with or be by quenched by hydrazides according to previously published work (*4*), the significance of this reaction in INH activation remains unknown and at present is considered of secondary importance. The yields of protein-based radicals in the absence of reducing substrate are significantly less than 1:1 compared to the yield of Compound I, which under these conditions is essentially quantitatively produced from the resting enzyme with excess PAA. Therefore, we focus only on the interaction between hydrazides and the catalytically competent oxoferryl−porphyrin π cation radical at this time. Previous work has also shown that in a biomimetic system, peroxidation (activation) of INH is quite efficient using very dilute hydrogen peroxide concentrations under conditions in which

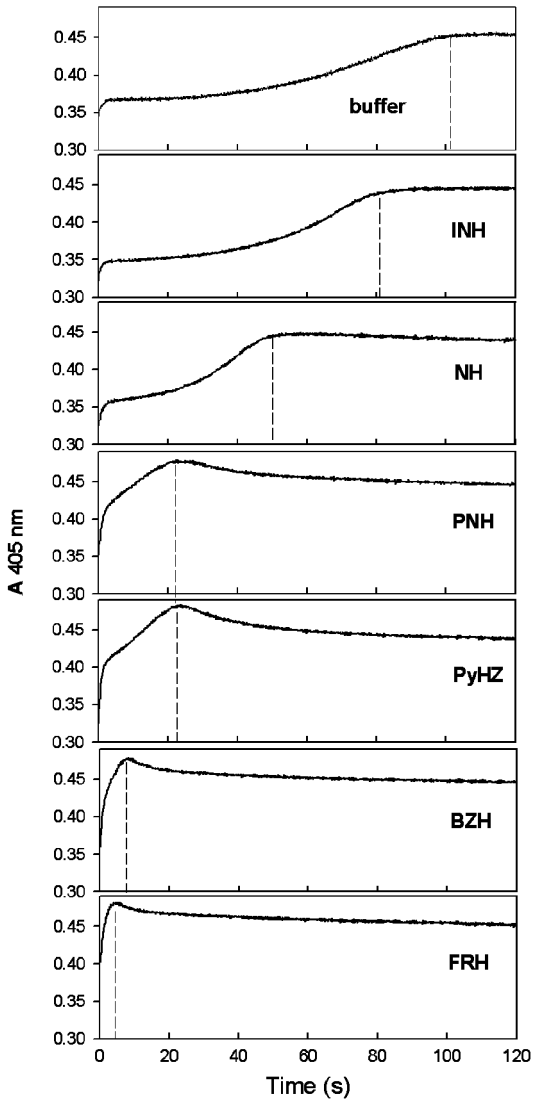

FIGURE 5: Stopped-flow study of reduction of KatG Compound I by hydrazides. Resting KatG was prereacted with PAA to form Compound I, followed by addition of hydrazides. The final concentrations of KatG, PAA, and hydrazides were 5, 50, and 50 μM, respectively. The KatG Soret absorbance at 405 nm was monitored immediately after the addition of hydrazide. Dashed lines indicate the points where the resting enzyme was fully restored.

protein-based radical production is considered to be negligible.] The Soret absorbance at 405 nm was monitored immediately after the second mixing step. As described in our previous study (*16*), the absorbance increase in the presence of INH and the other substrates is due to the return to the resting enzyme, which in the absence of reducing substrate takes approximately 2 min (due to endogenous electron transfer processes and formation of protein-based radicals). This return is accelerated by the hydrazides and also exhibits an overshoot due to the transient presence of 6-c heme iron as the majority enzyme form, which is the state of the enzyme upon completion of the peroxidase cycle. This species is transient, and new binding of hydrazide to the 6-c ferric enzyme restores the 5-c enzyme, which has a lower extinction coefficient as described above. The same set of aromatic hydrazides used in the binding studies with resting KatG was tested here. As shown in Figure 5, the rates of acceleration of the return to the resting absorbance caused by hydrazide reduction of Compound I are in the following order: FRH > BZH > PNH and PyHZ > NH > INH > buffer (which is the same order as the on rates for binding to resting enzyme). The amount of hydrazide we used here is far from the saturating amount according to our previously reported results (*16*), which allows the comparison of rates of different hydrazides at the same concentration. It is worth noting that the KatG enzyme in the Compound I form (regardless of its original coordination status in the resting state) is 6-c with an oxygen atom bound to iron, which resembles the 6-c KatG−fluoride complex in which high-affinity binding is prevented. Therefore, in KatG Compound I, INH may not have access to the identical high-affinity binding site as in the resting enzyme yet still reacts with this intermediate. The results observed here suggest that the rate of access of hydrazide to the heme pocket in the resting enzyme is also controlling the INH oxidation rate by Compound I.

It is interesting to note that INH, compared to NH and PNH, is the most potent antituberculosis drug but reacts with KatG with the slowest rates compared to the rates of these two ring isomers (and to all other hydrazides examined here). The antimycobacterial effect of INH involves the formation of an INH−NAD adduct that binds to and inhibits a key target enzyme, InhA. To verify whether the INH analogues form similar adducts through catalysis by KatG, the compounds were used as substrates in a protocol in which enzymatically generated hydrogen peroxide was used as an oxidant, in the presence of ferric KatG and NAD^+ (*10*). Of all the hydrazides that were tested, including those listed in Table 2, only INH and PNH generated the hydrazide−NAD adduct in this system. The yield of the PNH−NAD adduct was around 35% of that of the INH−NAD adduct (in 30 min), while BZH, PyNH, NH, and FRH failed to produce any detectable yields of adducts in our protocol. While the BZH−NAD adduct could be synthesized in good yield using manganese under aerobic conditions, and this adduct is an effective inhibitor of InhA (*14*), the efficiency of the activation reactions using KatG under the biomimetic conditions tried here was poor. This trend is consistent with the MIC values previously reported for these molecules (*34*).

DISCUSSION

Previous studies have demonstrated optical and EPR spectral changes in ferric KatG upon INH binding (*18*, *23*). In this study, we took advantage of quick binding INH analogues and could thereby collect reliable stoichiometry and kinetic parameters so that we could better understand the characteristics of INH binding. The most striking feature of the results is the hydrazide binding stoichiometry, which for freshly isolated KatG was found to be far less than equimolar with heme and also less than equimolar with protein dimer. Aged protein containing a large proportion of 6-c heme iron (along with 5-c heme species) binds more substrate with stoichiometries in some cases approaching one molecule per dimer. The binding profiles obtained in optical difference titrations correlated very well with the results from ITC studies, proving that only a subpopulation of the enzyme which is in a 6-c heme iron form exhibited a high affinity for these compounds.

The KatG enzyme and many mutants we have examined are in all cases isolated as a mixture of 5-c and 6-c heme

species in varying proportion, for reasons not yet understood. Six-coordinate KatG differs from 5-c protein most likely due to a water molecule weakly bound to heme iron (*10*), which according to the optical changes is displaced upon INH binding. Cyanide or fluoride complexes of KatG do not allow high-affinity binding of INH, which suggests steric interference even though INH does not directly coordinate to heme iron. Also, the mutants Y229F and W107F did not exhibit high-affinity binding to INH though they contain 6-c heme as the majority species (*25*). Therefore, it is not the six-coordination state of heme iron alone that provides for high-affinity binding. However, it is not yet clear what other structural differences exist between the different forms of the resting enzyme, especially surrounding the distal heme pocket and the substrate access channel that are associated with the 6-c species. Modifications in KatG in residues around the heme pocket or in the heme group itself (*10*, *21*, *22*, *32*) could be responsible for the specific changes that alter the INH binding interactions. These structural issues could be addressed in the future if methods for separately crystallizing and defining these species are developed.

In this study, we show that W107F or Y229F mutants lack high-affinity binding of INH. Previous GRID analysis suggested that energetically favorable interactions between INH and W107 and other distal residues (but not Y229) produce a potential INH binding site (*22*). Thus, a direct interaction between INH and the indole group of W107 is considered likely. It is noteworthy that the phenolic hydroxyl group of Y229 is facing in a direction opposite to the indole nitrogen of W107; it is thus unlikely that this group participates in hydrogen bonding with the hydrazide molecule. Both W107F and Y229F mutations disrupt formation of the triresidue (M255−Y229−W107) adduct. Therefore, the results suggest that the intact adduct on the distal site of the heme pocket provides the appropriate geometry for the high-affinity binding interactions in wild-type KatG and that neither side chain alone can produce the required specific interactions.

Another issue surrounding the distal side architecture is the fact that a modified indole nitrogen on W111 (W107 in *Mtb* KatG) was found in *Burkholderia pseudomallei* KatG, albeit in the structure of the enzyme analyzed from crystals after they were soaked very briefly at high pH (*35*, *36*). A modification was also found in the S324T mutant (*20*) of that enzyme and in *Mtb* KatG[S315T] at low pH (*10*). ITC results for titration of *Mtb* KatG at different pH values (5.5−8.5) did not, however, exhibit significant changes in INH binding stoichiometry or thermodynamics as might be expected if high-affinity binding required direct interaction with the indole nitrogen of W107. Furthermore, the optical absorbance of *Mtb* KatG, which was also used here to monitor hydrazide binding, did not exhibit noteworthy differences as a function of pH which argues against a change in heme iron coordination number or ligation state. Either, the pH-induced peroxy modification on W107 does not occur in WT *Mtb* KatG, or if it does, this modification has no effect on the optical spectrum or INH binding. Inconsistent with formation of such a modification is the fact that *Mtb* KatG, like *Sy* KatG, exhibits minimal NADH oxidase activity compared to *Bp* KatG in the same pH range. A direct association between such activity and the modification has been proposed by Carpena et al. (*35*).

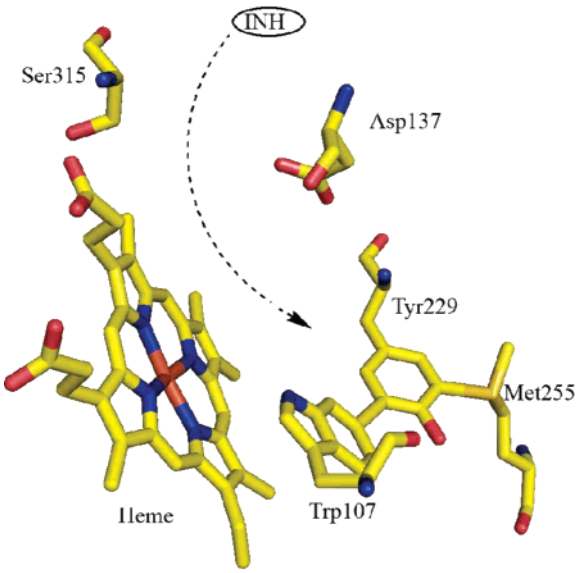

FIGURE 6: Structure of the distal heme pocket of *Mtb* KatG. This image was generated with PyMOL (*39*) using reported structures of *Mtb* WT KatG (PDB entry 2CCA). The arrow shows the access path of INH to the probable binding site.

Another notable phenomenon with regard to INH binding is the large ΔH value. As described above, the heat generated from slow substrate turnover would not follow the saturation profiles found both optically and by ITC. Thus, the enthalpy contribution from this kind of slow INH turnover is ruled out. When hydrazide binds, removal of the water molecule bound to heme iron alone would not give rise to a large enthalpy change. However, a change from 6-c to 5-c combined with a potential change in the spin state of the heme iron (*29*) could lead to an alteration in the proximal iron−His bond which would be transmitted to the rest of the subunit and the dimer, similar to the large-scale reorientation of hemoglobin subunits accompanying oxygen binding or dissociation. It is reasonable that rearrangement of hydrogen bond networks in the heme pocket and beyond could therefore account for the enthalpy change upon hydrazide binding. KatG adopts a very different solvent arrangement in the S315T mutant in the vicinity of the heme pocket and in the substrate access channel (*10*, *20*), and the structure of this mutant contains heme iron in a 5-c form. Thus, rearrangement of a collection of water molecules and formation of more stable hydrogen bonds between charged residues when INH binds to WT KatG could be rationalized.

Mutations in *Mtb* KatG have been found to affect INH binding, for example, for the mutant KatG[S315T] (*16*). How perturbation of INH binding affects drug activation needs to be analyzed on a case by case basis because steric and kinetic or mechanistic barriers could be involved. The S315T mutation, for example, narrows the substrate access channel and thereby limits the rate of peroxidation of INH (*37*) and also the rate of generation of the INH−NAD adduct (*10*, *11*). For mutants Y229F and W107F, only moderately reduced rates of INH−NAD adduct generation were found (∼40−60% of that of the wild-type enzyme). These mutations are located deep within the heme pocket (Figure 6), and apparently, a similar rate of turnover of INH may still occur in these mutants even though the specific binding interactions considered the origin of high-affinity binding in the resting wild-type enzyme are absent.

The thermodynamics of binding of INH to HRP has been reported (*31*); in that enzyme, INH binding results in a class II spectral change, consistent with coordination of a molecule of water rather than its dissociation as in KatG. The affinity of HRP for INH is in the millimolar range, while HRP has a much higher affinity for BHA; the opposite is true for KatG. Unlike HRP and P450 enzymes, the heme group of *Mtb* KatG is deeply buried at the bottom of a channel leading from the protein surface. This channel is narrowest near Ser315 and Asp137, where a 6 Å wide bottleneck is formed (*10*), which may contribute steric hindrance that leads to the slow binding of aromatic hydrazides.

These results shed light on the reasons why structural analogues of INH are not useful drugs. All the analogues tested here react more quickly with KatG Compound I than does INH and also bind more quickly to the resting enzyme, yet none of them (except for PNH) forms an NAD adduct analogous to the INH−NAD molecule in good yield. Even though all hydrazides are likely to form the same initial hydrazyl radical upon turnover with Compound I (*38*), the formation of adducts with NAD^+ is thought to depend on nonenzymatic acylation of the nicotinamide ring of NAD^+, and therefore, secondary features of this reaction come into play. It is likely that adduct formation requires acyl radicals sufficiently long-lived to diffuse off the enzyme and react with NAD^+. Thus, the nature of the ring substituent and the position and character of the heteroatom play key roles in the stabilization of radical intermediates required in the overall process of INH activation.

In conclusion, aromatic hydrazide substrates bind to only a small portion of WT *Mtb* KatG, which is a 6-c species containing an easily dissociated sixth heme iron ligand. These findings can provide guidelines for substrate selection and maximization of binding stoichiometry for future crystallization studies. The complete description of a well-defined INH binding site in KatG awaits further study.

ACKNOWLEDGMENT

We thank Feng Wang and Dr. James C. Sacchettini (Texas A&M University, College Station, TX) for stimulating discussions during this research.

SUPPORTING INFORMATION AVAILABLE

Absorption spectra of freshly prepared KatG and aged KatG, alone with the corresponding spectra after INH titration are provided. This material is available free of charge via the Internet at http://pubs.acs.org.

REFERENCES

1. Middlebrook, G., Cohn, M. L., and Schaeffer, W. B. (1954) *Am. Rev. Tuberc. 70*, 852−872.
2. Zhang, Y., Heym, B., Allen, B., Young, D., and Cole, S. (1992) The catalase-peroxidase gene and isoniazid resistance of *Mycobacterium tuberculosis*, *Nature 358*, 591−593.
3. Chouchane, S., Lippai, I., and Magliozzo, R. S. (2000) Catalase-peroxidase (*Mycobacterium tuberculosis* KatG) catalysis and isoniazid activation, *Biochemistry 39*, 9975−9983.
4. Chouchane, S., Girotto, S., Yu, S., and Magliozzo, R. S. (2002) Identification and Characterization of Tyrosyl Radical Formation in *Mycobacterium tuberculosis* Catalase-Peroxidase (KatG), *J. Biol. Chem. 277*, 42633−42638.
5. Ivancich, A., Jakopitsch, C., Auer, M., Un, S., and Obinger, C. (2003) Protein-based radicals in the catalase-peroxidase of synechocystis PCC6803: A multifrequency EPR investigation of wild-type and variants on the environment of the heme active site, *J. Am. Chem. Soc. 125*, 14093−14102.
6. Jakopitsch, C., Obinger, C., Un, S., and Ivancich, A. (2006) Identification of Trp106 as the tryptophanyl radical intermediate in *Synechocystis* PCC6803 catalase-peroxidase by multifrequency electron paramagnetic resonance spectroscopy, *J. Inorg. Biochem. 100*, 1091−1099.
7. Ghiladi, R. A., Cabelli, D. E., and Ortiz de Montellano, P. R. (2004) Superoxide reactivity of KatG: Insights into isoniazid resistance pathways in TB, *J. Am. Chem. Soc. 126*, 4772−4773.
8. Johnsson, K., and Schultz, P. G. (1994) Mechanistic studies of the oxidation of isoniazid by the catalase-peroxidase from *Mycobacterium tuberculosis*, *J. Am. Chem. Soc. 116*, 7425−7426.
9. Lei, B., Wei, C. J., and Tu, S. C. (2000) Action mechanism of antitubercular isoniazid. Activation by *Mycobacterium tuberculosis* KatG, isolation, and characterization of inha inhibitor, *J. Biol. Chem. 275*, 2520−2526.
10. Zhao, X., Yu, H., Yu, S., Wang, F., Sacchettini, J. C., and Magliozzo, R. S. (2006) Hydrogen peroxide-mediated isoniazid activation catalyzed by *Mycobacterium tuberculosis* catalase-peroxidase (KatG) and its S315T mutant, *Biochemistry 45*, 4131−4140.
11. Ghiladi, R. A., Medzihradszky, K. F., Rusnak, F. M., and Ortiz de Montellano, P. R. (2005) Correlation between Isoniazid Resistance and Superoxide Reactivity in *Mycobacterium tuberculosis* KatG, *J. Am. Chem. Soc. 127*, 13428−13442.
12. Johnsson, K., King, D. S., and Schultz, P. G. (1995) Studies on the mechanism of action of isoniazid and ethionamide in the chemotherapy of tuberculosis, *J. Am. Chem. Soc. 117*, 5009−5010.
13. Rozwarski, D. A., Grant, G. A., Barton, D. H. R., Jacobs, W. R., Jr., and Sacchettini, J. C. (1998) Modification of the NADH of the isoniazid target (InhA) from *Mycobacterium tuberculosis*, *Science 279*, 98−102.
14. Rawat, R., Whitty, A., and Tonge, P. J. (2003) The isoniazid-NAD adduct is a slow, tight-binding inhibitor of InhA, the *Mycobacterium tuberculosis* enoyl reductase: Adduct affinity and drug resistance, *Proc. Natl. Acad. Sci. U.S.A. 100*, 13881−13886.
15. Argyrou, A., Vetting, M. W., Aladegbami, B., and Blanchard, J. S. (2006) *Mycobacterium tuberculosis* dihydrofolate reductase is a target for isoniazid, *Nat. Struct. Mol. Biol. 13*, 408−413.
16. Yu, S., Girotto, S., Lee, C., and Magliozzo, R. S. (2003) Reduced Affinity for Isoniazid in the S315T Mutant of *Mycobacterium tuberculosis* KatG Is a Key Factor in Antibiotic Resistance, *J. Biol. Chem. 278*, 14769−14775.
17. Todorovic, S., Juranic, N., Macura, S., and Rusnak, F. (1999) Binding of ^{15}N-labeled isoniazid to KatG and KatG(S315T): Use of two-spin [zz]-order relaxation rate for ^{15}N-Fe distance determination, *J. Am. Chem. Soc. 121*, 10962−10966.
18. Wengenack, N. L., Todorovic, S., Yu, L., and Rusnak, F. (1998) Evidence for differential binding of isoniazid by *Mycobacterium tuberculosis* KatG and the isoniazid-resistant mutant KatG(S315T), *Biochemistry 37*, 15825−15834.
19. Pierattelli, R., Banci, L., Eady, N. A. J., Bodiguel, J., Jones, J. N., Moody, P. C. E., Raven, E. L., Jamart-Gregoire, B., and Brown, K. A. (2004) Enzyme-catalyzed Mechanism of Isoniazid Activation in Class I and Class III Peroxidases, *J. Biol. Chem. 279*, 39000−39009.
20. Deemagarn, T., Carpena, X., Singh, R., Wiseman, B., Fita, I., and Loewen, P. C. (2005) Structural characterization of the Ser324Thr variant of the catalase-peroxidase (KatG) from *Burkholderia pseudomallei*, *J. Mol. Biol. 345*, 21−28.
21. Carpena, X., Loprasert, S., Mongkolsuk, S., Switala, J., Loewen, P. C., and Fita, I. (2003) Catalase-peroxidase KatG of *Burkholderia pseudomallei* at 1.7 Å resolution, *J. Mol. Biol. 327*, 475−489.
22. Bertrand, T., Eady, N. A. J., Jones, J. N., Jesmin, Nagy, J. M., Jamart-Gregoire, B., Raven, E. L., and Brown, K. A. (2004) Crystal Structure of *Mycobacterium tuberculosis* Catalase-Peroxidase, *J. Biol. Chem. 279*, 38991−38999.
23. Wengenack, N. L., Lane, B. D., Hill, P. J., Uhl, J. R., Lukat-Rodgers, G. S., Hall, L., Roberts, G. D., Cockerill, F. R., III, Brennan, P. J., Rodgers, K. R., Belisle, J. T., and Rusnak, F. (2004) Purification and characterization of *Mycobacterium tuberculosis* KatG, KatG(S315T), and *Mycobacterium bovis* KatG(R463L), *Protein Expression Purif. 36*, 232−243.

24. Chouchane, S., Girotto, S., Kapetanaki, S., Schelvis, J. P., Yu, S., and Magliozzo, R. S. (2003) Analysis of heme structural heterogeneity in *Mycobacterium tuberculosis* catalase-peroxidase (KatG), *J. Biol. Chem. 278*, 8154−8162.
25. Yu, S., Girotto, S., Zhao, X., and Magliozzo, R. S. (2003) Rapid Formation of Compound II and a Tyrosyl Radical in the Y229F Mutant of *Mycobacterium tuberculosis* Catalase-peroxidase Disrupts Catalase but Not Peroxidase Function, *J. Biol. Chem. 278*, 44121−44127.
26. Magliozzo, R. S., and Marcinkeviciene, J. A. (1996) Evidence for isoniazid oxidation by oxyferrous mycobacterial catalase-peroxidase, *J. Am. Chem. Soc. 118*, 11303−11304.
27. Falk, J. K. (1964) *Porphyrin and Metalloporphyrins*, Elsevier Publishing Co., New York.
28. Wengenack, N. L., Hoard, H. M., and Rusnak, F. (1999) Isoniazid Oxidation by *Mycobacterium tuberculosis* KatG: A Role for Superoxide Which Correlates with Isoniazid Susceptibility, *J. Am. Chem. Soc. 121*, 9748−9749.
29. Kapetanaki, S., Chouchane, S., Girotto, S., Yu, S., Magliozzo, R. S., and Schelvis, J. P. (2003) Conformational differences in *Mycobacterium tuberculosis* catalase-peroxidase KatG and its S315T mutant revealed by resonance Raman spectroscopy, *Biochemistry 42*, 3835−3845.
30. Kapetanaki, S. M., Chouchane, S., Yu, S., Zhao, X., Magliozzo, R. S., and Schelvis, J. P. (2005) *Mycobacterium tuberculosis* KatG(S315T) catalase-peroxidase retains all active site properties for proper catalytic function, *Biochemistry 44*, 243−252.
31. Aitken, S. M., Turnbull, J. L., Percival, M. D., and English, A. M. (2001) Thermodynamic analysis of the binding of aromatic hydroxamic acid analogues to ferric horseradish peroxidase, *Biochemistry 40*, 13980−13989.
32. Yamada, Y., Fujiwara, T., Sato, T., Igarashi, N., and Tanaka, N. (2002) The 2.0 Å crystal structure of catalase-peroxidase from *Haloarcula marismortui*, *Nat. Struct. Biol. 9*, 691−695.
33. Schreiber, G., and Fersht, A. R. (1996) Rapid, electrostatically assisted association of proteins, *Nat. Struct. Biol. 3*, 427−431.
34. Klopman, G., Fercu, D., and Jacob, J. (1996) Computer-aided study of the relationship between structure and antituberculosis activity of a series of isoniazid derivatives, *Chem. Phys. 204*, 181.
35. Carpena, X., Wiseman, B., Deemagarn, T., Herguedas, B., Ivancich, A., Singh, R., Loewen, P. C., and Fita, I. (2006) Roles for Arg426 and Trp111 in the modulation of NADH oxidase activity of the catalase-peroxidase KatG from *Burkholderia pseudomallei* inferred from pH-induced structural changes, *Biochemistry 45*, 5171−5179.
36. Deemagarn, T., Wiseman, B., Carpena, X., Ivancich, A., Fita, I., and Loewen, P. C. (2007) Two alternative substrate paths for compound I formation and reduction in catalase-peroxidase KatG from *Burkholderia pseudomallei*, *Proteins 66*, 219−228.
37. Wengenack, N. L., Uhl, J. R., St Amand, A. L., Tomlinson, A. J., Benson, L. M., Naylor, S., Kline, B. C., Cockerill, F. R., III, and Rusnak, F. (1997) Recombinant *Mycobacterium tuberculosis* KatG(S315T) is a competent catalase-peroxidase with reduced activity toward isoniazid, *J. Infect. Dis. 176*, 722−727.
38. Wengenack, N. L., and Rusnak, F. (2001) Evidence for isoniazid-dependent free radical generation catalyzed by *Mycobacterium tuberculosis* KatG and the isoniazid-resistant mutant KatG(S315T), *Biochemistry 40*, 8990−8996.
39. Delano, W. L. (2004) *The PyMol Molecular Graphics System*, DeLano Scientific, San Carlos, CA.

BI062218P